Dark soliton collisions in a toroidal Bose-Einstein condensate

D. M. Jezek,[1] P. Capuzzi,[1,2] and H. M. Cataldo[1]

[1] *IFIBA-CONICET*

[2] *Departamento de Física, Facultad de Ciencias Exactas y Naturales, Universidad de Buenos Aires, Pabellón 1, Ciudad Universitaria, 1428 Buenos Aires, Argentina*

Abstract

We study the dynamics of two gray solitons in a Bose-Einstein condensate confined by a toroidal trap with a tight confinement in the radial direction. Gross-Pitaevskii simulations show that solitons can be long living objects passing through many collisional processes. We have observed quite different behaviors depending on the soliton velocity. Very slow solitons, obtained by perturbing the stationary solitonic profile, move with a constant angular velocity until they collide elastically and move in the opposite direction without showing any sign of lowering their energy. In this case the density notches are always well separated and the fronts are sharp and straight. Faster solitons present vortices around the notches, which play a central role during the collisions. We have found that in these processes the solitons lose energy, as the outgoing velocity turns out to be larger than the incoming one. To study the dynamics, we model the gray soliton state with a free parameter that is related to the soliton velocity. We further analyze the energy, soliton velocity and turning points in terms of such a free parameter, finding that the main features are in accordance with the infinite one-dimensional system.

PACS numbers: 03.75.Lm, 03.75.Hh, 03.75.Kk

I. INTRODUCTION

Topological defects has been a central topic in nonlinear systems of various fields in physics. In Bose-Einstein condensates (BECs), such defects include vortices, solitons and solitonic vortices (svortices). Solitons are characterized by their form stability under time evolution and can behave akin to classical particles. For a repulsive interaction between atoms, black solitons are stationary states with a π jump in the phase of the order parameter, which produces a density nodal surface. In contrast, gray solitons are moving objects with a nonvanishing density dip, characteristic of a smaller phase difference between both sides of the density notch. In an infinite one-dimensional (1D) system the collision of solitons has been thoroughly studied from the theoretical viewpoint [1–4]. It has been shown that for soliton speeds smaller (larger) than half the sound velocity, the solitons remain separated (overlapped) at the collision, appearing to be *reflected* by (*transmitted* through) each other [4]. In such a system the solitons collide elastically and continue moving with a constant velocity away from the collision region. In particular, for very slow solitons the system can be safely regarded as hard-sphere-like particles that interact through an effective (velocity dependent) repulsive potential [4].

On the other hand, vortices are characterized by a quantized circulation of the velocity field around the position where the density vanishes. Svortices [5] are present in tightly confined systems, and differ from standard vortices in the form of their density distribution which looks quite similar to the soliton one, although the velocity field changes its sign along the density dip, where the vortex is located.

Solitons in atomic BECs confined with different trapping potential geometries have been extensively studied in the last years [6, 7]. And renewed interest has arisen from the experimental observation of solitonic vortices in bosonic and fermionic systems [8–10]. In such recent BEC experiments, solitons have been spontaneously created through the Kibble-Zurek mechanism [11].

The commonly used candidate to experimentally study the soliton dynamics in a quasi 1D system has been a cigar-shaped condensate [12]. However, due to the harmonic trapping potential, such a single soliton dynamics differs considerably with respect to that of the strictly 1D case, where the soliton moves with a constant speed. That is, in the Thomas-Fermi approximation a soliton oscillates in a cigar-shaped condensate with a frequency

$\omega_s = \omega_{trap}/\sqrt{2}$ [4, 13–15], where ω_{trap} is the angular frequency of the trap in the longitudinal direction, a result that can be interpreted in terms of the definition of the soliton mass [16]. It is worthwhile noticing that one can avoid such a potentially undesirable effect stemming from the harmonic trap by utilizing a toroidal-shaped condensate. However, only few works have undertaken the study of soliton dynamics in toroidal condensates including the possible formation of svortices [17, 18].

The aim of this work is to study the double-notch soliton dynamics occurring in a toroidal BEC, which involves many collisional processes with a related vortex dynamics. In Section II we introduce the system, particularly the toroidal trap and the set of parameters involved. In Section III, first we numerically obtain by solving the stationary Gross-Pitaevskii (GP) equation the black soliton order parameter. In a second step, based on the 1D black soliton profile we construct gray solitons with imprinted velocities which range from very slow values up to velocities near the ground-state sound speed. By solving the time-dependent GP equation, we study in Section IV the dynamics of such gray solitons, observing that there exist two different regimes depending on the type of collision involved and the role played by vortices. Section V is devoted to the analysis of the energy, soliton velocity and turning points, where we discuss their behavior in comparison to that of the infinite 1D system. Finally, the conclusions of our study are gathered in Section VI.

II. THE SYSTEM

The trapping potential is written as the sum of a term $V_{\rm RG}$ that depends on the radial coordinate $r = \sqrt{x^2 + y^2}$ and gives rise to the toroidal shape of the condensate, and a term that is harmonic in the z direction:

$$V_{\rm trap}(x, y, z) = V_{\rm RG}(r) + \frac{1}{2} M \omega_z^2 z^2 \,, \tag{1}$$

where M denotes the atomic mass of ^{87}Rb and ω_z is the trap frequency in the z-direction. The potential term that confines the atoms in the radial direction is modeled as the following ring-Gaussian potential [19]

$$V_{\rm RG}(r) = -V_0 \, \exp\left[-\Lambda \left(\frac{r}{r_0} - 1\right)^2\right], \tag{2}$$

where V_0 and r_0 denote the depth and radius of its minimum. The dimensionless parameter Λ is associated to the $1/e^2$ width ($w = r_0\sqrt{\frac{2}{\Lambda}}$) of such a ring-Gaussian potential.

The trap parameters have been selected according to the experimental conditions of Ref. [20]. We have set V_0=70 nK, $r_0 = 4$ μm, and we will work with a fixed particle number $N = 3000$. We will further assume a high value of $\omega_z = 2\pi \times 921.77$ Hz, yielding a quasi two-dimensional condensate that allows a simplified numerical treatment [21]. Then, the order parameter can be represented as a product of a wave function on the x-y plane $\psi(x, y)$, and a Gaussian wave function along the z coordinate from which the following effective two-dimensional interacting parameter can be extracted [21]

$$g = g_{3D} \left(\frac{M\omega_z}{2\pi\hbar} \right)^{1/2}, \tag{3}$$

where $g_{3D} = 4\pi\hbar^2 a/M$, $a = 98.98\, a_0$ being the s-wave scattering length of ^{87}Rb and a_0 the Bohr radius. The value of the remaining dimensionless parameter $\Lambda = 20$ ($w = 1.265$ μm) was chosen to assure also a tightly confined condensate in the radial direction. However, we have not simplified our treatment to a 1D system because, as we will see, vortices play an interesting role in the dynamics. Finally, it is worth mentioning that henceforth all the order parameters will be normalized to the number of particles.

III. DARK SOLITONS

A. Black soliton

To obtain the exact GP black soliton order parameter, we numerically seek for a state which exhibits uniform phases at both sides of a nodal straight line with a π jump between them. We note that, expressed as a function of the angle θ defined along the torus, such an order parameter presents two density notches located at $\theta = 0$ and $\theta = \pi$, and thus can be treated as a two-soliton system. The structure of such a state is in accordance with the 1D picture, in which dark solitons interact with each other via a repulsive potential [4]. In fact, one expects that in a stationary configuration both solitons should be separated from each other by the largest distance compatible with the constraints, which in this case corresponds to diametrically opposite positions along the ring. We have numerically calculated the GP order parameter of this double-notch soliton by applying an imaginary time method to an initial state given by the ground state order parameter with an imprinted phase difference of π between the half-planes delimited by the x axis. The resulting solution of the stationary

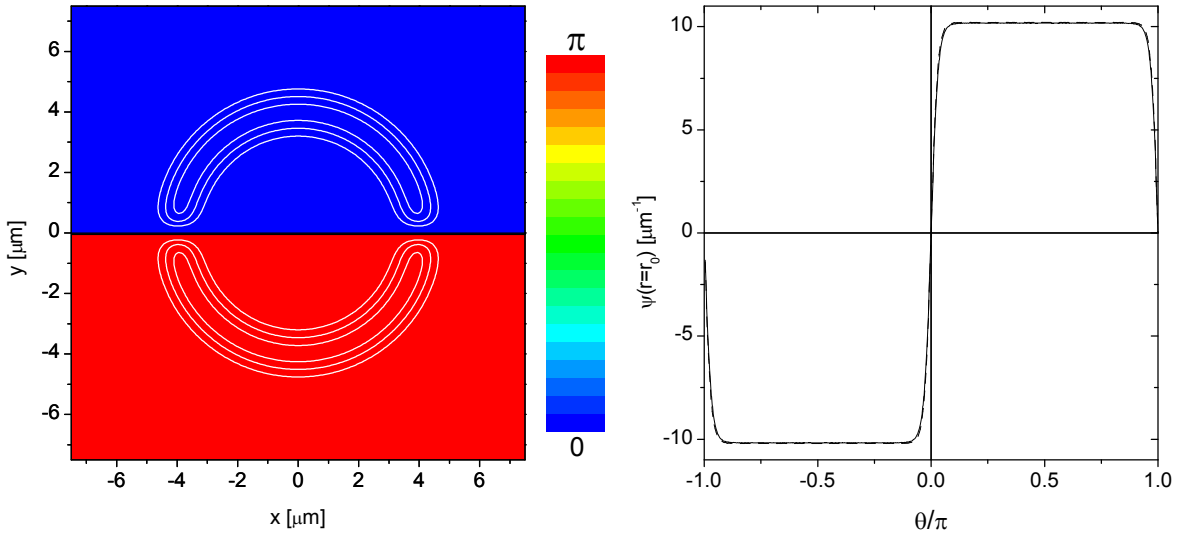

FIG. 1. (Color online) Black soliton isodensity contour (solid white lines) and phase distribution (colors) are shown in the left panel. The GP order parameter (solid line) and the almost superposed results from Eq. (4) with $f(r = r_0) = 1$ and $k = 2.785\ \mu\text{m}^{-1}$ (dotted line) are displayed on the right panel.

GP equation presents a nodal line along the x axis, preserving the phase difference of π. In Fig. 1 we show the corresponding phase distribution and isodensity contour (left panel), along with the real order parameter as a function of θ at $r = r_0$ (solid line, right panel).

Due to the tight confinement in the radial direction, one expects that the double-notch black soliton should present a similar profile in the angular direction to that of the two-node stationary analytic solution in a strictly 1D ring system, which is given in terms of Jacobi elliptic functions [22]. As stated in such reference, since the zeros of the solution are well separated the analytic behavior near such points approaches a hyperbolic tangent function. This is in fact so for our two-dimensional order parameter, since it may be safely modeled by

$$\psi_B(r, \theta) = \sqrt{n}\, f(r) \tanh(kr \sin\theta), \tag{4}$$

where n denotes the maximum value of the particle density, k a parameter of the order of the inverse of the healing length, and $f(r)$ represents a function to be determined. Particularly, in the right panel of Fig. 1, we may appreciate the agreement with the GP result for $f(r = r_0) = 1$ and the value $k = 2.785\ \mu\text{m}^{-1}$ which will be obtained in the following subsection.

B. Gray soliton

To study the solitonic dynamics we may construct a gray soliton order parameter by introducing an imaginary part in the black soliton state (4). More precisely, in analogy with the 1D case [1], we propose dynamical states of the form,

$$\psi_G(r,\theta) = \sqrt{n}\ f(r)[\sqrt{1-X^2}\tanh(\sqrt{1-X^2}\,kr\sin\theta) + iX]\,. \tag{5}$$

We note that for a very large torus radius, one can associate the above state to infinite 1D solitons moving in the $y = r\sin\theta$ direction with velocity $v_s = cX$, c being the sound speed [1].

Due to the lack of an analytical expression for $f(r)$, we shall adopt three different proposals in order to minimize possible residual excitations that could arise at different ranges of the soliton depth, however, we will show that the corresponding results do not differ significantly from each other. The first proposal consists in dividing the GP black soliton order parameter by $\tanh(kr\sin\theta)$, next multiplying the result obtained by $\sqrt{1-X^2}\tanh(\sqrt{1-X^2}kr\sin\theta) + iX$, and finally renormalizing to N, which we shall call a perturbed black soliton (PBS) state. The second state, which we will call perturbed ground (PG) state, comes from repeating the above procedure with the ground-state wavefunction instead of the black soliton one and omitting the division step. We expect these approximate order parameters should work satisfactorily not far from $X = 0$ ($X = 1$) for the PBS (PG) state.

By inspection of the radial dependence of the order parameters of both ground and black soliton states, we have found that they can be approximately modeled with a Gaussian profile. Then, to cover a wider range of X values, we propose a third choice that reproduces such a radial dependence. We thus assume the following order parameter,

$$\psi_{GM}(r,\theta) = \sqrt{n(X)}\,\exp\left[-\frac{\gamma}{2}\left(1-\frac{r}{r_0}\right)^2\right]\,\left[\sqrt{1-X^2}\tanh\left(\sqrt{1-X^2}\,kr\sin\theta\right) + iX\right], \tag{6}$$

which, choosing an adequate value of γ, fits quite well the radial profile of the GP density, both for the black soliton ($X = 0$) and the ground state ($X = 1$), as can be seen in Fig. 2. We will call this state as the Gaussian model (GM) state.

We note that we have included the function $n(X)$ in the GM order parameter in view that in a finite system, in contrast to an infinite one, the existence of a hole in the condensate density increases the density maximum with respect to that of the ground state. We may

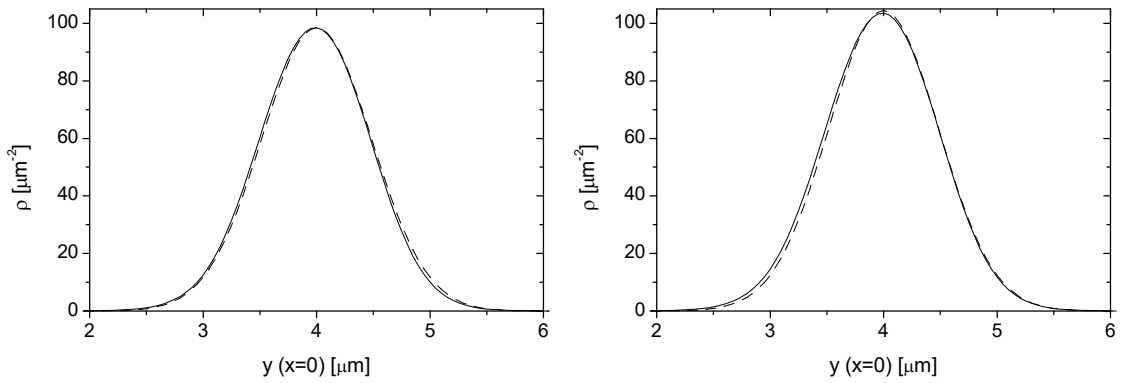

FIG. 2. Density profiles ρ as functions of the radial coordinate for the ground (left panel) and black soliton (right panel) states. Solid lines correspond to the GP density, whereas dashed lines correspond to $\rho_{GM} = |\psi_{GM}|^2$, where ψ_{GM} is given by Eq. (6) with $\gamma = 34$, for $X = 1$ (left panel) and $X = 0$ (right panel).

obtain an analytical expression for $n(X)$ by incorporating the constraint that the number of particles for each X value should be equal to that of the ground state. In doing so, due to the tight confinement in the radial direction and the fact that the width of the notch is much smaller than the diameter of the torus, in the integral of the density $\rho_{GM} = |\psi_{GM}(r,\theta)|^2$ we may safely replace $r\sin\theta$ by $r_0\,\theta$ inside the argument of the hyperbolic function. We have verified that such an approximation introduces an error in the integral of less than one percent. Then, under such assumptions we obtain the following condition,

$$n(X) = \frac{n_0}{1 - \frac{2\sqrt{1-X^2}}{\pi k r_0}}, \tag{7}$$

where n_0 denotes the ground-state density maximum located at $r = r_0$, which is fitted to the GP value.

The remaining parameter k can be estimated by applying the stationary GP equation to the black soliton state (6), which evaluated at $r = r_0$ yields

$$k = \frac{\sqrt{n(X=0)gM}}{\hbar}, \tag{8}$$

which turns out to be the inverse of the local healing length at $r = r_0$. Therefore, combining Eq. (7) for $X = 0$ and Eq. (8), we obtain the value $k = 2.785\ \mu\text{m}^{-1}$.

Finally, we note that the usage of $n(X)$ in the GM order parameter for calculating the density, turns out to be important to accurately describe the density maximum for every X

value in comparison to GP simulations, as can be observed for $X = 1$ at the right panel of Fig. 2.

IV. THE DYNAMICS

To study the soliton dynamics, we have solved the time-dependent GP equation using as an initial order parameter any of the three alternatives described in the previous section. By varying the parameter X, which is associated to the initially imprinted soliton velocity, we have observed different dynamics that show a transition around $X = 0.5$.

A. Soliton reflection at the collision ($0 < X < 0.5$)

For small values of X corresponding to low velocities of the defect, solitons remain as long living objects, whose dynamics presents almost constant velocity, except for very narrow time intervals when the collisions occur. In this case the collisions seem to be elastic. On the other hand, the presence of vortices is only observed far away from the condensate, and they do not play any role in the soliton dynamics. In general, our findings are quite similar to those of the homogeneous 1D system. In Fig. 3 we show the results of GP simulations for a PBS initial order parameter with a small imprinted velocity obtained with $X = 0.01$. The angular position $\theta(t)$ of the soliton located at positive x values is depicted at the left panel. It may be seen that the absolute value of the slope of $\theta(t)$ is almost the same throughout the evolution, except for small intervals around the turning points. Hence the soliton energy, which depends on its speed, seems to be conserved. Another signature of such a conservation comes from the fixed positions of the turning points that remain located at $\theta = \pm 0.37008\,\pi$. On the other hand, in the right panel we depict the phase difference between the upper and lower regions separated by the notches. Specifically, we have evaluated such a phase difference as $\Delta\phi = \phi(x = 0, y = 4\,\mu\text{m}) - \phi(x = 0, y = -4\,\mu\text{m})$. One can observe that $\Delta\phi(t)$ alternates between values near $-\pi$ and π in the intervals of increasing and decreasing angles, respectively.

With such an initial state, which is very close to the stationary black soliton, one finds that the system evolves with quite pure solitonic fronts. In Fig. 4 we show three snapshots of phase and particle density around the first collision (or turning point). In the top-right

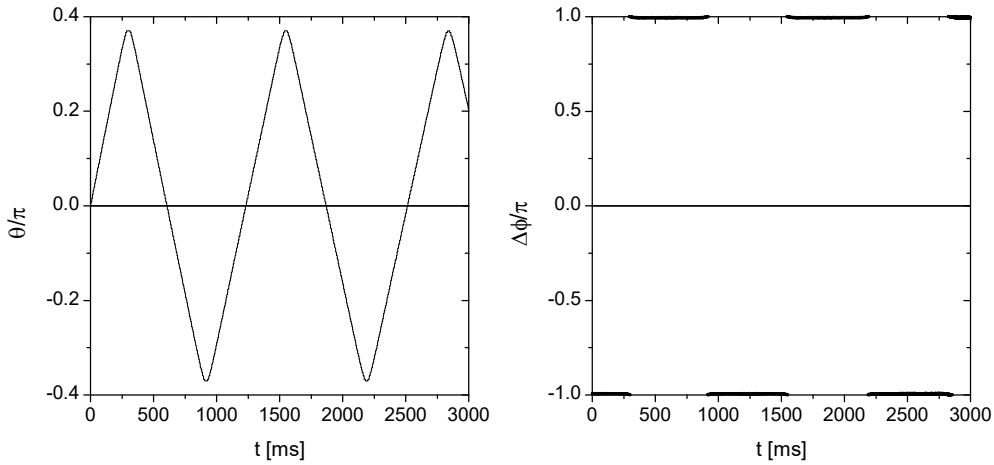

FIG. 3. Angular position (left panel) of the soliton located at $x > 0$ and the phase difference $\Delta\phi$ (right panel), are depicted as functions of the time using an initial PBS profile with the black soliton slightly perturbed with $X = 0.01$.

panel, one observes that before the collision the phase gradient is almost zero, except in small regions around the dips, where it points in the opposite direction to the soliton velocity. And, as expected, only few particles situated at the borders of the notch move in this opposite direction. In the middle-right panel, it may be seen that during the collision the density maintains two well separated notches, whose minima go to zero, which is characteristic of a vanishing soliton velocity corresponding to a real order parameter with a phase difference of π. At such a turning point, the velocity field is zero even around the notch, as seen from the vanishing phase gradient everywhere, except for the phase discontinuity where the density vanishes. Finally, after the collision the velocity field is reversed and the soliton continues moving in the opposite direction, as shown at the bottom panels.

For larger X values we do not observe such pure solitonic fronts, since the phase accumulation distributed along each notch now spreads around a vortex state. Such combined soliton-vortex quasiparticles are usually called solitonic vortices or svortices [5]. We have found that these vortices move with the soliton angular velocity along a circular trajectory of a radius slightly larger than r_0, except near the zone where the collision takes place, where they perform a complicated dynamics. In Fig. 5 we show the results of a GP simulation using an initial GM order parameter given by Eq. (6) with $X = 0.1$. The angular position of the soliton located at $x > 0$ (left panel) and the phase difference $\Delta\phi$ (right panel), are

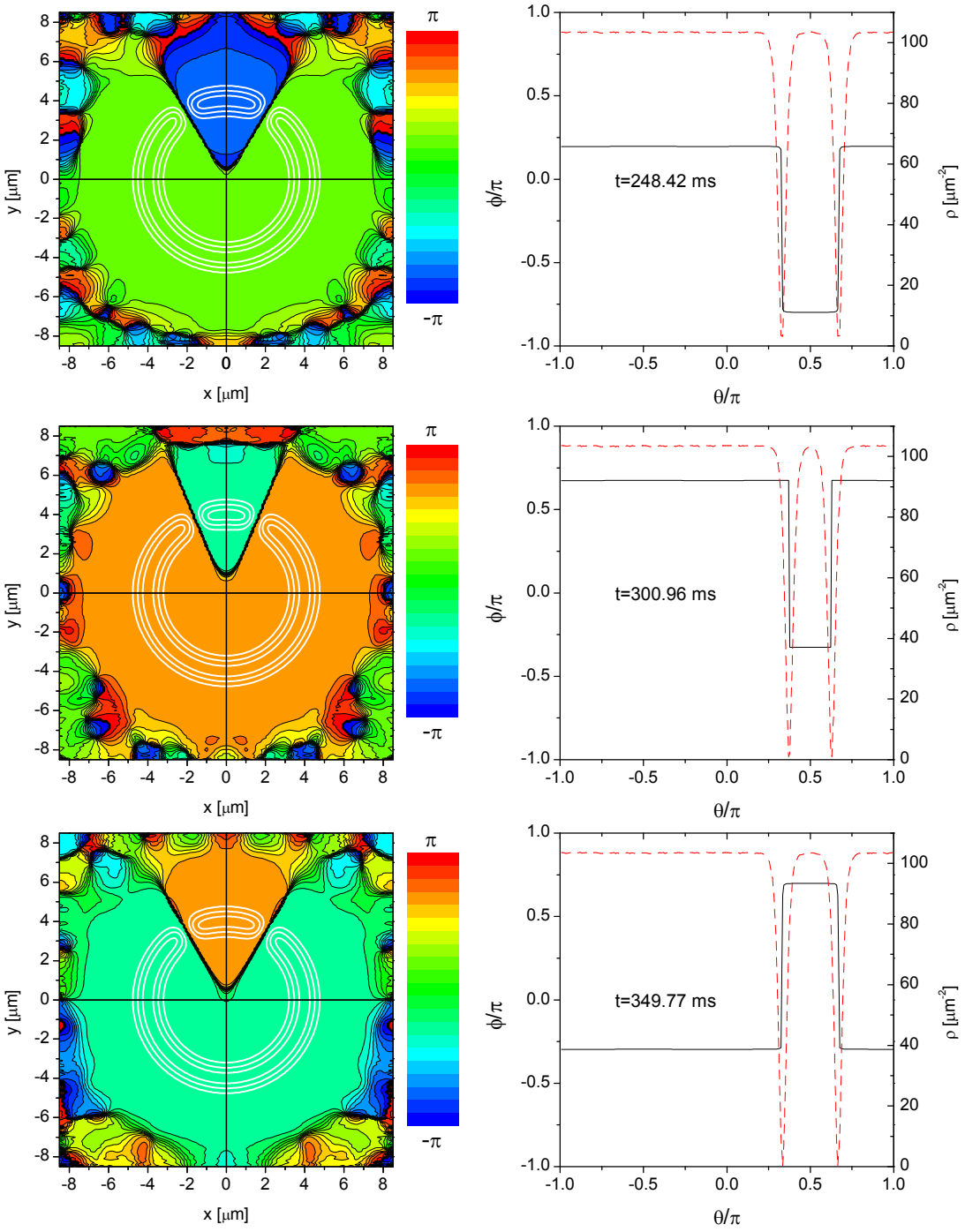

FIG. 4. (Color online) Snapshots before (top panels), during (middle panels), and after (bottom panels) the first soliton collision for the same initial state of Fig. 3. In the left panels we show the phase distribution (colors) and density isocontours (white solid lines), while in the right panels we depict the corresponding angular distribution of particle density (red dashed line) and phase (black solid line) at $r = 4\,\mu$m.

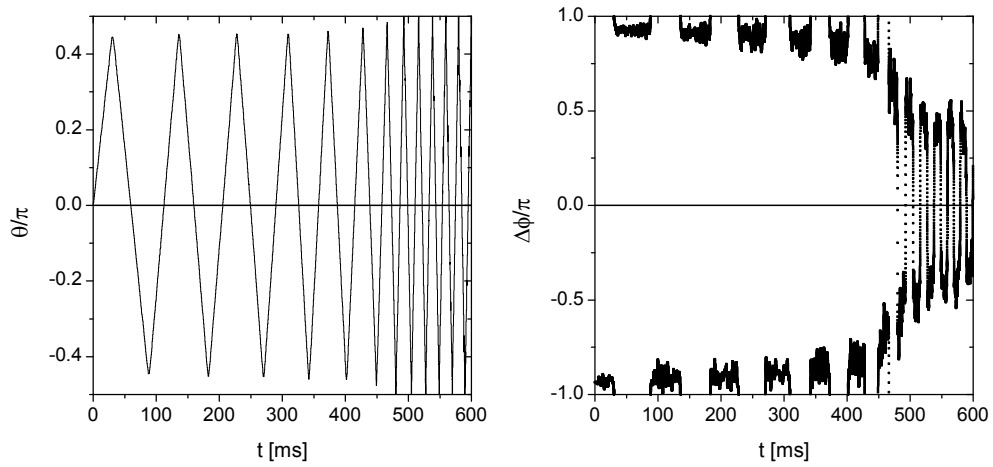

FIG. 5. Angular position (left panel) of the soliton located at $x > 0$ and the phase difference $\Delta\phi$ (right panel), are depicted as functions of the time using the initial GM profile given by Eq. (6) with $X = 0.1$.

depicted as functions of time. We observe an increasing absolute value of the slope of $\theta(t)$ after each collision. Also the maximum absolute value θ_M of the angle θ keeps growing along the evolution. For example, for the first and third collision we obtained $\theta_M/\pi = 0.44485$ and $\theta_M/\pi = 0.4514$, respectively. After many oscillations, at $t \simeq 470$ ms when $\theta_M/\pi = 0.5$ is attained, it may be seen that the system enters a different regime that will be described in the next subsection. Such a transition occurs when the soliton exceeds a critical velocity $v_c \simeq 0.8\,\mu$m/ms.

In Fig. 6 we show snapshots of the phase and particle density around the first collision for different times. It may be seen that in the collision time (middle panels), the density presents two well separated notches forming an angle $\Delta\theta \simeq 0.11\pi$. In this case, the passage of vortices along the notches, in the radial direction, is responsible for the velocity field inversion, as also has been observed in the self-trapping regime for a double-well system, where the vortices move along the junction [23]. In particular, the velocity field inversion in this collision may be produced by either the motion along the notch of an external ($r > r_0$) counterclockwise vortex in the negative radial direction, which is the present case, or by an inner ($r < r_0$) clockwise vortex, passing through the notch towards the outside region. We note that such a dynamics has no physical analogue in pure 1D systems as they are vortex-free. In the top-left panel of Fig. 6, we may see that before the collision the vortex associated with the soliton at the right has a counterclockwise vorticity and, as it is located

at $r > r_0$, the net flux of particles across the corresponding density notch points clockwise, as expected. On the other hand, after the collision (bottom-left panel), the new arising vortex presents a clockwise vorticity, consistent with the change of direction of the velocity field. A similar behavior has been observed for the different initial conditions up to soliton velocities around v_c.

Finally we want to note that in the presence of vortices, the density does not necessarily vanish during the collision at $r = r_0$, as seen in the middle-right panel of Fig. 6. One can only assure that the density vanishes at the points where the vortices are located. As can also be observed from the right panels of Fig. 6, one has $|\Delta\phi| \simeq \pi$ at the collision (middle panel), whereas before and after the collision smaller values of $|\Delta\phi|$ are obtained. In addition, the change of sign that $\Delta\phi$ undergoes between the upper an lower panels is consistent with the inversion of the soliton velocity.

B. Soliton transmission at the collision ($0.5 < X < 1$)

As we have pointed out in the previous subsection, for velocities larger than $v_c \simeq 0.8\,\mu$m/ms the system enters a different regime. And in fact, for $X > 0.5$, we have found that the initial soliton velocity exceeds v_c, and thus the whole evolution lies within this regime. Similarly to what happens in infinite 1D systems for $v_s/c > 0.5$ [4], we shall see that in such a regime the solitons can be thought of as being transmitted through each other, as they completely overlap during the collision. We recall that in infinite 1D systems a single notch of vanishing density is produced at the collisions with $v_s/c = 0.5$ [4, 7], which is characteristic of a double root of a real order parameter preserving the same sign on the overall space. Whereas for $v_s/c > 0.5$, such a single notch has a nonvanishing density and the colliding solitons have been interpreted as transmitting through each other [4]. It is worthwhile mentioning that in experimental works on bright solitons [24], it has been shown that the solitons pass through one another and emerge from the collision unaltered in shape, amplitude, or velocity, but with a new trajectory. Similar qualitative features have been observed in our case, but this time accompanied with an associated vortex dynamics. However, it is important to note that we have found that the soliton velocity slightly increases during the evolution, becoming after many collisions appreciably larger than the initial value.

In the left panel of Fig. 7, we show the angular position of the soliton located at $x > 0$

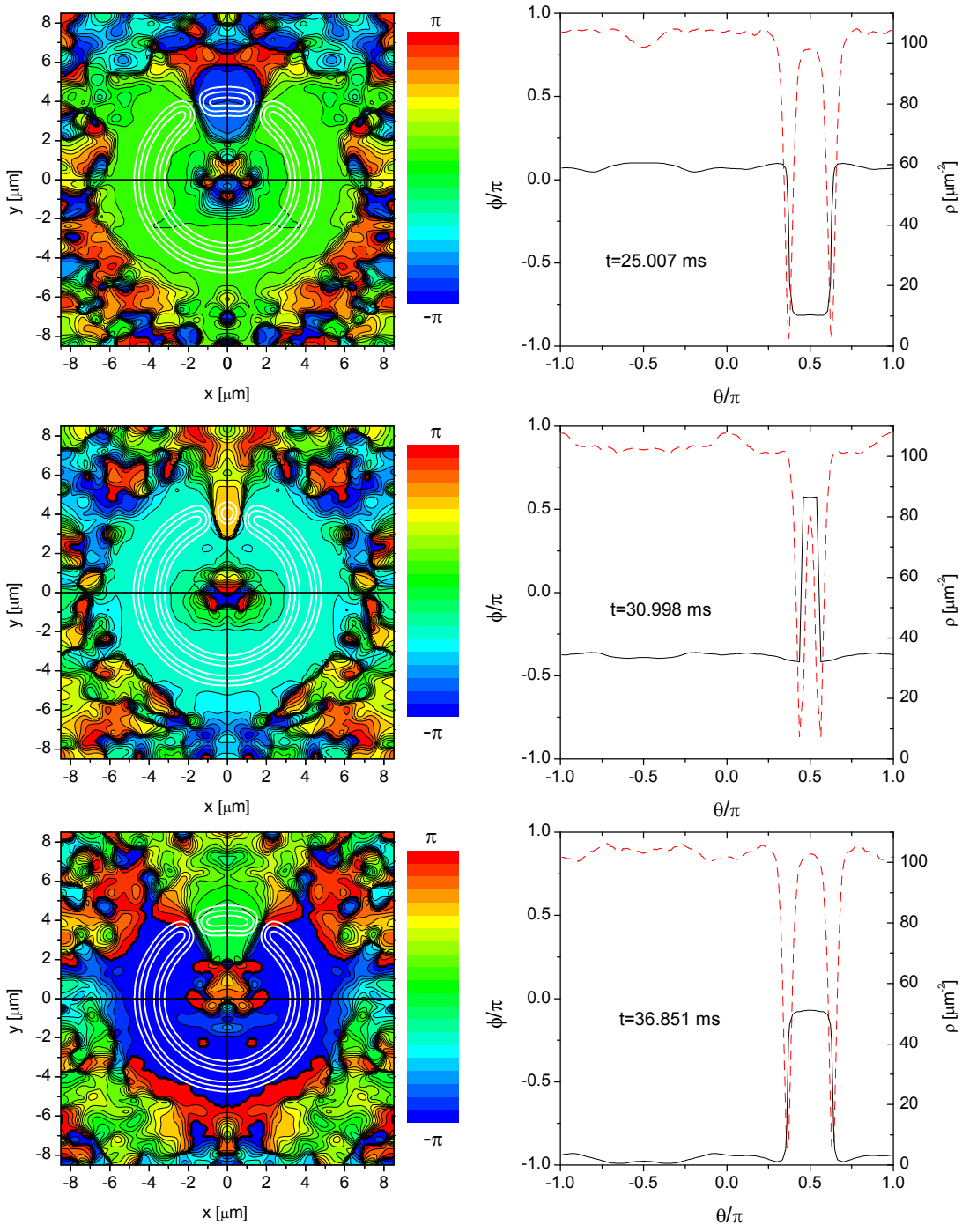

FIG. 6. (Color online) Snapshots before (top panels), during (middle panels), and after (bottom panels) the first soliton collision for the same initial state of Fig. 5. In the left panels we show the phase distribution (colors) and density isocontours (white solid lines), while in the right panels we depict the corresponding angular distribution of particle density (red dashed line) and phase (black solid line) at $r = 4\,\mu$m.

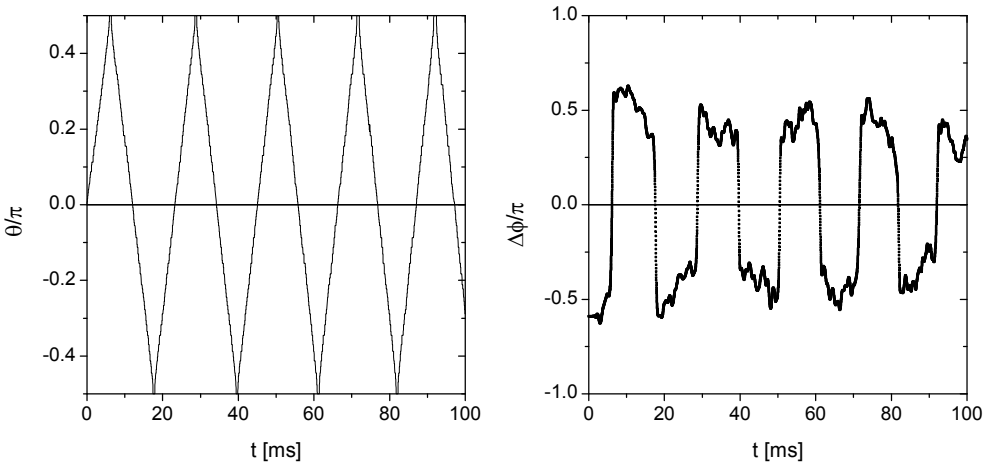

FIG. 7. Angular position (left panel) of the soliton located at $x > 0$ and the phase difference $\Delta\phi$ (right panel), are depicted as functions of the time for an initial GM profile given by Eq. (6) with $X = 0.6$.

as a function of time for $X = 0.6$, where it may be seen that at each collision the maximum absolute value reaches the value $\pi/2$, which means that both solitons approach each other until they completely overlap just at the collision time.

On the other hand, the time evolution of the phase difference is shown at the right panel of Fig. 7, where we may observe that in contrast to the regime with $v_s < v_c$, the phase difference remains bounded. Particularly, one can estimate such an upper bound from the formula $v_s/c = \cos(\Delta\phi/2)$ derived for an infinite 1D system, assuming that the transition occurs for $v_s = 0.5\,c$ which yields $\Delta\phi/\pi = 2/3$, a value that agrees very well with that observed at the right panel of Fig. 5. Moreover, just at the collision time, the phase difference also shows a quite distinct behavior for solitons moving slower or faster than the critical velocity. That is, we have observed that $|\Delta\phi|$ reaches the value π at collisions with $v_s < v_c$, whereas it goes to zero for soliton velocities above such a value. This behavior is clearly shown on the right panels of Figs. 5 and 7.

The dynamics in this regime is again ruled by vortices, which precede around the condensate, except near the collision, where once more a complex vortex dynamics takes place. It can be seen in the top-left panel of Fig. 8, that the vortices are located farther from the center than in the previous case, which is in accordance with a larger vortex velocity [25], as the soliton also moves faster.

During the collision we have observed the annihilation of the vortex and the antivortex coming with each soliton. The counterclockwise vortex at $x > 0$, viewed at the top-left panel, annihilates with the clockwise vortex located at $x < 0$. In fact, in the middle-left panel it may be seen that both vortices have completely disappeared. Just after the collision, a new vortex-antivortex pair is generated at each notch. The vortex and antivortex forming the pair rapidly separate from each other, as can be seen in the bottom-left panel of Fig. 8, and from analyzing subsequent times, we have observed that the inner vortex becomes absorbed towards the central region. On the other hand, the outer vortices with vorticities opposite to those before the collision, keep ruling the soliton dynamics.

By comparing the right panels of Fig. 8, it can be seen that the density reaches the minimum, yet nonvanishing, value at the collision time (middle panel) when the notches completely overlap. On the other hand, $\Delta\phi$ changes its sign between the upper and lower panels, while the phase is almost uniform in the middle one, yielding $\Delta\phi = 0$.

Finally we want to note that our numerical results are consistent with the fact that faster solitons have smaller depths, as can be seen from the density plots of the right panels of Figs. 6 and 8.

V. DEPENDENCE OF THE PHYSICAL QUANTITIES ON X

In this section we will study the dependence on X of the initial soliton energy and velocity, and also the position of turning points at the collisions, comparing all these results to the infinite 1D case. It is worthwhile mentioning that we will disregard the presence of vortices in the analytical calculations.

A. Energy

We first recall that in an infinite 1D system, the single dark soliton order parameter has an analytical expression which is characterized by the parameter $X = v_s/c$ [1, 6, 7]. In addition, it is easy to verify that the associated energy can be written as $E_{1D} = (4/3)\hbar n_0 c(1 - X^2)^{3/2}$ [6, 7, 15], where n_0 denotes the background density.

In this subsection we will study the dependence on X of the double-notch soliton energy for the PBS, GM and PG initial states. In particular, for the GM order parameter (given

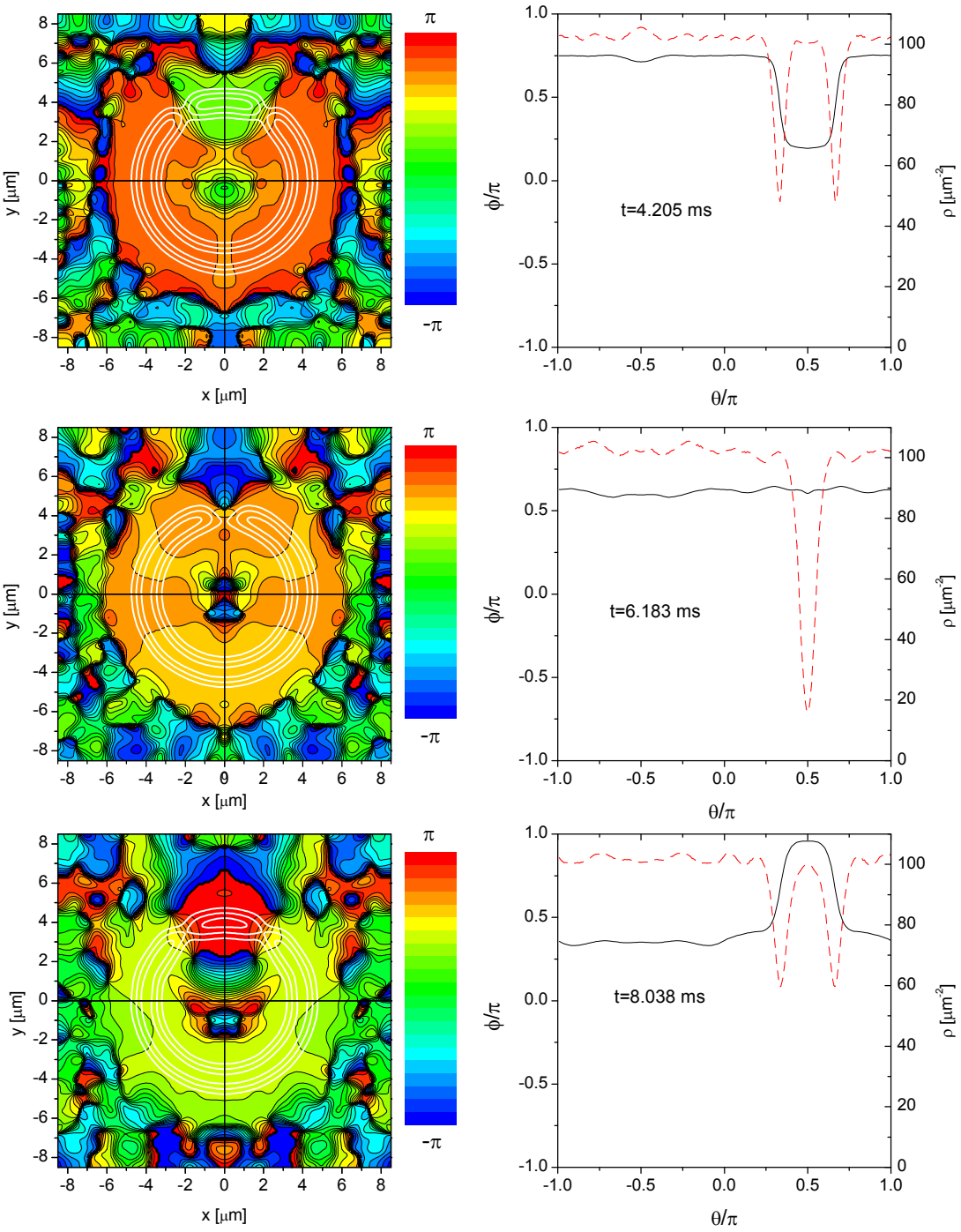

FIG. 8. (Color online) Snapshots before (top panels), during (middle panels), and after (bottom panels) the first soliton collision for the same initial state of Fig. 7. In the left panels we show the phase distribution (colors) and density isocontours (white solid lines), while in the right panels we depict the corresponding angular distribution of particle density (red dashed line) and phase (black solid line) at $r = 4\,\mu$m.

by Eq. (6)), we may also obtain an expression for the energy by performing the same type of approximations in the integrals as we have done to derive Eq. (7). Taking into account such considerations, we may finally obtain the soliton energy by evaluating the kinetic, trap and interaction energy terms, and then subtracting the ground state energy (E_0),

$$E_S(X) = E(X) - E_0 \simeq \frac{4(1+\sqrt{2})}{3\sqrt{2}} \frac{g\, n(X)^2 B}{k r_0} (1-X^2)^{3/2} - \frac{4}{\pi\sqrt{2}} \frac{g\, n(X)^2 B}{(k r_0)^2} (1-X^2) \quad (9)$$

where $B = r_0^2\sqrt{\pi/\gamma}$. We observe a similar dependence on X to the infinite 1D case, but it is important to stress that in this case we do not have such a simple relation between X and the soliton velocity.

In Fig. 9 we display our numerical calculations of the energy per particle, together with the estimate arising from Eq. (9). Note that for X approaching zero (unity), the energy should be better described by the PBS (PG) order parameter. In this context, we observe that the energy arising from the GM order parameter (6) and the corresponding estimate (9) accurately reproduce the PG results. We also show in Fig. 9 the X dependence of the 1D soliton energy E_{1D}, which turns out to be qualitatively similar to that arising from Eq. (9).

B. Soliton velocity

Here we will analyze the relation between the parameter X and the initial soliton velocity. To elucidate whether we can assign to the parameter X the same physical meaning as in the infinite 1D case, namely the ratio between soliton and sound speeds, we depict in Fig. 10 the soliton velocity before the first collision as a function of X. We recall that as seen in the previous section, the soliton speed may increase along the time evolution. However, it is worthwhile noticing that the soliton velocities before the first collision turn out to be quite similar for the three different kinds of initial order parameters. We have also plotted in Fig. 10 the linear functions $f_i(X) = c_i X$, where c_i is an estimate of the sound velocity obtained by tracking the motion of a small localized density perturbation, in either the ground or the black soliton states, which yielded $c_0 = 1.52\,\mu$m/ms and $c_1 = 1.6\,\mu$m/ms, respectively. Such functions $f_i(X)$ represent estimates of the soliton velocity assuming a linear dependence on X as predicted for an infinite 1D system, using both extremes c_i of the sound velocity. We want to remark that as the size of the condensate is finite, the

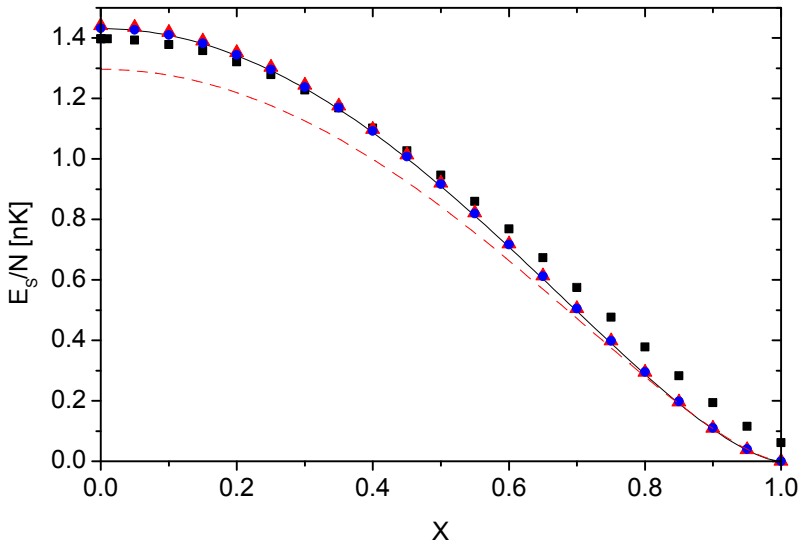

FIG. 9. (Color online) Soliton energy per particle as a function of X. The solid black line corresponds to Eq. (9); the black squares, blue circles, and red triangles correspond to numerical calculations using PBS, GM, and PG states, respectively. The red dashed line corresponds to an infinite 1D system.

background density changes with the depth of the notch, and thus the sound velocity also varies. In particular, the sound velocity of the ground (black soliton) state turns out to be the smallest (largest) one. Therefore, for any intermediate X value, the sound velocity $c(X)$ should verify $c_0 \leq c(X) \leq c_1$.

From the results depicted in Fig. 10, we may certainly conclude that the parameter X can roughly be approximated by the ratio of the soliton velocity and a mean sound speed between c_0 and c_1. A possible source of discrepancy in this respect could arise from the fact that even before the first collision, the soliton velocity undergoes a gradual growth due to energy dissipation. In addition, for large soliton velocities the presence of vortices may also be affecting the results.

It is worth to notice that, as can be seen in Fig. 10, within the dispersion of data given by the different approaches, the soliton velocity lies around $v \simeq 0.8 \mu m/ms$ for $X = 0.5$, which is consistent with the classification of the dynamics we have performed using either $X < 0.5$ or $X > 0.5$.

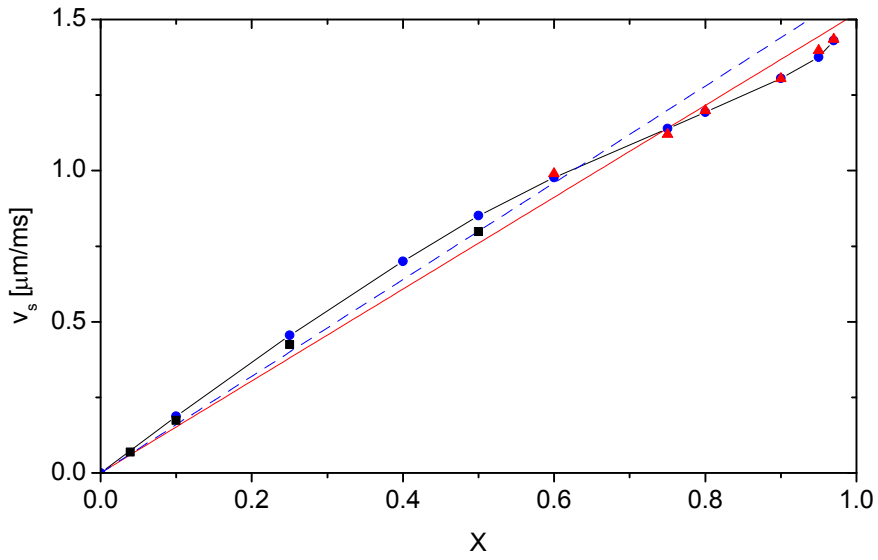

FIG. 10. (Color online) The soliton initial velocity for the PBS (black squares), GM (blue circles), and PG (red triangles) states depicted as a function of X. The black solid line has been drawn to guide the eye on the GM results. The linear functions $c_i X$ are depicted as a red solid line ($i = 0$) and as a dashed blue line ($i = 1$), where c_i is an estimate of the sound velocity at either the ground ($i = 0$) or the black soliton ($i = 1$) states.

C. Turning points

In a linear homogeneous 1D system, the turning points for low speed solitons ($X = v_s/c \leq 1/2$) have been calculated analytically [4], yielding the following expression for the minimum distance d reached in a symmetric collision:

$$d = \frac{\zeta}{\sqrt{1-X^2}} \cosh^{-1}(\frac{1}{X} - 2X), \tag{10}$$

where ζ denotes the healing length.

Assuming one may apply formula (10) to our toroidal configuration to estimate the turning angle θ_M for the first collision of the soliton located at $x > 0$, one obtains

$$\theta_M = \frac{\pi}{2} - \frac{1}{2kr_0\sqrt{1-X^2}} \cosh^{-1}(\frac{1}{X} - 2X), \tag{11}$$

whose results are depicted in Fig. 11. In the same figure we show the corresponding GP simulation results using the GM order parameter as the initial state. We do not depict the points arising from PBS and PG states because the three approaches threw practically

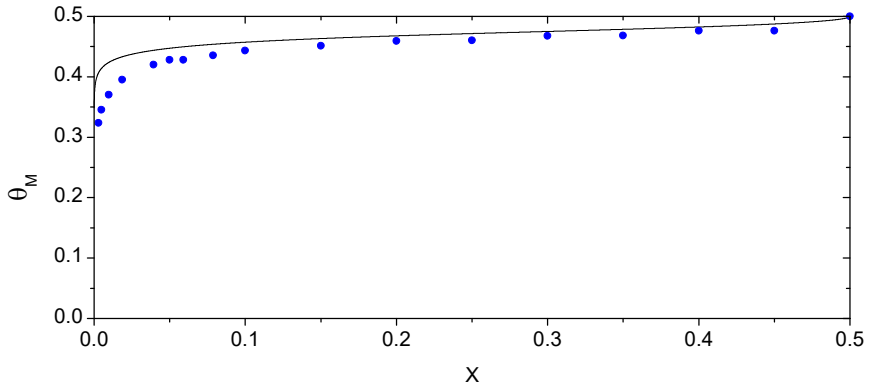

FIG. 11. The turning points arising from GP simulations using the GM order parameter (blue circles) and the estimate given by Eq. (11) (black solid line) are depicted as a function of X.

the same results. By comparing the solid line with the distribution of points, a qualitative similar behavior is observed, with a discrepancy that may be adjudicated to the difference in the geometry between the torus and an infinite 1D system.

Finally, we note that a repulsive potential between solitons, from which an estimate for the turning points can be derived, has been proposed for the 1D system in the limit $X \ll 1/2$ [4]. Assuming that such a potential also rules the dynamics of our system, we derived another estimate of the turning angle, which yielded practically the same results of Eq. (11) for $X \lesssim 0.2$.

VI. CONCLUSIONS

We have observed quite different characteristics of the collision processes depending on the soliton velocities. For very slow speeds, the solitons remain as long living defects whose dynamics presents almost constant velocities, except within a narrow region where the collision takes place. In this process, the colliding solitons lower their velocity to zero and continue moving in the opposite direction with the same speed that had before the collision. Therefore, such an event can be considered as an elastic collision, and hence, in energy terms, the soliton dynamics seems to be non dissipative. On the other hand, the turning points are always located at the same angle during the time evolution, with well separated notches and fronts sharp and straight. There is no evidence of vortex generation near the condensate that can affect the soliton dynamics.

For faster solitons, the dynamics is ruled by vortices which define svortices structures. Such vortices precede around the condensate, except within a small region where the collision takes place, where they perform a more complex dynamics around the notches. In these processes the solitons lose energy, as the outgoing velocity turns out to be larger than the incoming one.

For soliton speeds smaller than approximately half the sound velocity, the density dips remain separated during the collision and the passage of vortices along each notch, in the radial direction, causes the inversion of the local velocity field. We find that the angular distance of closest proximity between the colliding solitons decreases with the increasing soliton velocity. Taking into account that the notches are well separated during the collision, in accordance with the infinite 1D case [4] we may say that the solitons are reflected by each other. However it is important to recall that the outgoing vortex has the opposite circulation to the incoming one.

A different regime arises for soliton speeds larger than around half the sound velocity. Namely, as in the 1D case [4], the density dips become completely overlapped at the collision and the solitons are transmitted through each other. In this case the vortex dynamics during the collision turns out to be simpler than in the preceding case, since the vortices that come from each soliton front annihilate with each other, and afterwards new vortices are generated that start ruling the subsequent dynamics.

As a general remark we want to notice that, as we have seen in most cases, during the evolution the soliton increases its velocity and thus reduces its energy. It is then natural to wonder where such a released energy is being transferred, given that it is well known that the time-dependent GP equation conserves the energy of the entire system. From the analysis of the whole dynamics, we have observed that such a soliton energy dissipation is accompanied by an increasing number of vortices that become gathered together in the inner region of the torus, along with the appearance of a large amount of density fluctuations. These excitations may be viewed, at an early stage, in the left panels of Figs. 6 and 8. Hence, we may conclude that part of the initial soliton energy is being transferred to the increasing number of vortices and density fluctuations.

From the study of the energy, soliton velocity and turning points before the onset of dissipation, we have found that the behaviors of these quantities as functions of X qualitatively resemble those of the infinite 1D case for $X = v_s/c$.

Finally, we wish to point out that a corresponding experimental set up of our system seems to be definitely within the reach of the present investigations. Particularly, the toroidal condensate we have proposed has already been experimentally achieved [20], while our solitonic initial profiles could eventually be generated by standard phase and/or density manipulation methods [16].

Note added. After the initial submission of this paper a preprint appeared [26] where the authors show the feasibility of experimental generation of counter-propagating solitons, moving at velocities above half the sound speed in a similar toroidal geometry.

ACKNOWLEDGMENTS

PC acknowledges financial support from ANCyPT through Grant No. PICT 2011-01217. HMC acknowledges CONICET for financial support under Grant No. PIP 11420100100083.

[1] T. Tsuzuki, J. Low Temp. Phys. **4**, 441 (1971).

[2] V. E. Zakharov and A. B. Shabat, Zh. Eksp. Teor. Fiz. **64**, 1627 (1973), [Sov. Phys. JETP **37**, 823 (1973)].

[3] L. P. Pitaevskii and S. Stringari, *Bose-Einstein Condensation* (Oxford University Press, Oxford, 2003).

[4] G. Theocharis, A. Weller, J. P. Ronzheimer, C. Gross, M. K. Oberthaler, P. G. Kevrekidis, and D. J. Frantzeskakis, Phys. Rev. A **81**, 063604 (2010).

[5] J. Brand and W. P. Reinhardt, Phys. Rev. A **65**, 043612 (2002).

[6] V. V. Konotop, in *Emergent Nonlinear Phenomena in Bose-Einstein Condensates* (Springer-Verlag, Heidelberg, 2008) pp. 65–83.

[7] D. J. Frantzeskakis, J. Phys. A: Math. Theor. **43**, 213001 (2010).

[8] S. Donadello, S. Serafini, M. Tylutki, L. P. Pitaevskii, F. Dalfovo, G. Lamporesi, and G. Ferrari, Phys. Rev. Lett. **113**, 065302 (2014).

[9] M. J. H. Ku, W. Ji, B. Mukherjee, E. Guardado-Sanchez, L. W. Cheuk, T. Yefsah, and M. W. Zwierlein, Phys. Rev. Lett. **113**, 065301 (2014).

[10] F. Chevy, Physics **7**, 82 (2014).

[11] G. Lamporesi, S. Donadello, S. Serafini, F. Dalfovo, and G. Ferrari, Nature Phys. **9**, 656 (2013).

[12] S. Burger, K. Bongs, S. Dettmer, W. Ertmer, K. Sengstock, A. Sanpera, G. V. Shlyapnikov, and M. Lewenstein, Phys. Rev. Lett **83**, 5198 (1999).

[13] P. O. Fedichev, A. E. Muryshev, and G. V. Shlyapnikov, Phys. Rev. A **60**, 3220 (1999).

[14] T. Busch and J. R. Anglin, Phys. Rev. Lett **84**, 2298 (2000).

[15] V. V. Konotop and L. Pitaevskii, Phys. Rev. Lett. **93**, 240403 (2004).

[16] C. Becker, S. Stellmer, P. Soltan-Panahi, S. Dörscher, M. Baumert, E. M. Richter, J. Kronjäger, K. Bongs, and K. Sengstock, Nature Phys. **4**, 496 (2008).

[17] J. Brand and W. P. Reinhardt, J. Phys. B: At. Mol. Opt. Phys. **34**, L113 (2001).

[18] A. Muñoz Mateo, A. Gallemí, M. Guilleumas, and R. Mayol, Phys. Rev. A **91**, 063625 (2015).

[19] N. Murray, M. Krygier, M. Edwards, K. C. Wright, G. K. Campbell, and C. W. Clark, Phys. Rev. A **88**, 053615 (2013).

[20] C. Ryu, P. W. Blackburn, A. A. Blinova, and M. G. Boshier, Phys. Rev. Lett. **111**, 205301 (2013).

[21] Y. Castin and R. Dum, Eur. Phys. J. D **7**, 399 (1999).

[22] L. D. Carr, C. W. Clark, and W. P. Reinhardt, Phys. Rev. A **62**, 063610 (2000).

[23] M. Abad, M. Guilleumas, R. Mayol, M. Pi, and D. M. Jezek, Phys. Rev. A **84**, 035601 (2011); M. Abad, M. Guilleumas, R. Mayol, F. Piazza, D. M. Jezek, and A. Smerzi, Europhys. Lett. **109**, 40005 (2015).

[24] J. H. V. Nguyen, P. Dyke, D. Luo, B. A. Malomed, and R. G. Hulet, Nature Phys. **10**, 918 (2014).

[25] H. M. Cataldo and D. M. Jezek, Eur. Phys. J. D **54**, 585 (2009); D. M. Jezek and H. M. Cataldo, Phys. Rev. A **77**, 043602 (2008).

[26] D. Gallucci and N. P. Proukakis, (2015), arXiv:1510.07078.